A Restorable, Variable Stiffness Pneumatic Soft Gripper Based on Jamming of Strings of Beads

Fenglin Han, Lei Fei, Run Zou, Weijian Li, Jinghao Zhou, and Haiming Zhao

***Abstract*—Soft robots based on particle jamming cannot return to the initial position and initial mechanical state due to the accumulation of particles after removing the particle jamming, which means poor restorability, and the compliance of the robots during deformation will be reduced because of the jamming effect. Here, we present the design, fabrication, and tests of a novel soft actuator with good restorability and compliance. To improve the restorability of the actuator, we used cotton threads to connect the spherical acrylic beads into form strings instead of discrete beads. The beads could be pulled to the initial position by the threads, the actuator also returns to the initial state. To avoid the jamming effect during the deformation of the actuator, we used compressed air to drive the actuator and injected the beads into the actuator after the active deformation. To reduce the driving pressure and facilitate the flow of the beads, an initial noncontact, frame-type strain constraint structure was designed for the soft actuator. Experimental data show that the actuator was flexible during bending and the stiffness can increase more than 12-fold to resist the external load. By pulling the threads, the actuator could be restored to the initial state with an error of less than 3% of the actuator length after an operation cycle. The soft gripper based on the actuator can grasp repeatedly or laterally. The gripper can grasp soft objects such as a piece of tofu and a balloon of water, and the maximum weight that can be stably grasped is 2.744 kg.**

***Index Terms*—Grippers and other end-effectors, particle jamming, soft robot applications, soft robot materials and design.**

I. Introduction

SOFT robotics is a burgeoning technology to expand the capability of robots because of its excellent environmental adaptability [1], [2]. Soft material endows robots with substantial compliance, while weakening their weight-bearing capacity.

Manuscript received 25 March 2023; accepted 21 May 2023. Date of publication 7 June 2023; date of current version 4 October 2023. This work was supported in part by the Natural Science Foundation of Hunan Province, China under Grant 2020JJ4706 and in part by the Science and Technology Innovation Program of Hunan Province under Grant 2022GK4027. This paper was recommended for publication by Associate Editor C. Sung and Editor M. Yim upon evaluation of the reviewers' comments. *(Corresponding author: Haiming Zhao.)*

Fenglin Han and Haiming Zhao are with the State Key Laboratory of Precision Manufacturing for Extreme Service Performance, Central South University, Changsha 410083, China, and also with the College of Mechanical and Electrical Engineering, Central South University, Changsha 410083, China (e-mail: hanfl@csu.edu.cn; zhm0097@126.com).

Lei Fei, Run Zou, Weijian Li, and Jinghao Zhou are with the College of Mechanical and Electrical Engineering, Central South University, Changsha 410083, China (e-mail: xiangcaidd@foxmail.com; zourun2r@163.com; 452795753@qq.com; 1290791042@qq.com).

This article has supplementary material provided by the authors and color versions of one or more figures available at https://doi.org/10.1109/TRO.2023.3280595.

Digital Object Identifier 10.1109/TRO.2023.3280595

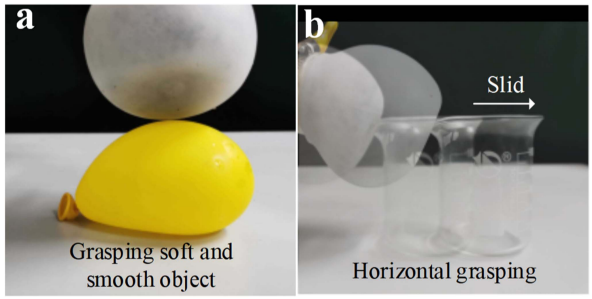

Fig. 1. Performance of the universal gripper. (a) Lateral grab. (b) Grasping soft objects.

This contradiction limits the practicality and universality of soft robots. Variable stiffness technology can make the stiffness of the robot adjust on a large range and has therefore become a research focus in the soft robotics community [3].

There are numerous methods to achieve variable stiffness, such as antagonist [4], [5], material phase changing [6], [7], layer jamming [8], [9], [10], and particle jamming [11], [12], [13], [14]. Compared with other methods, the soft actuator using particle jamming has better adaptability to the object's contact shape and is easier to implement. Thus, many researchers use particle jamming to improve the stiffness of soft robots, especially soft grippers [15].

The jamming-based soft grippers are mainly divided into two types: universal grippers based on a spherical soft membrane and multifinger grippers based on soft actuators. Brown et al. [16] developed a universal gripper, which was the first application of particle jamming in the stiffness control of soft structures. Subsequently, improved designs based on the universal gripper have been developed, which can grasp objects with different shapes, sizes, and weights [17], [18]. For example, researchers proposed to use positive pressure to remove the jamming effect and release the object. With the positive pressure, the soft membrane can restore to its original state, and the gripper can grasp repeatedly [19], [20]. However, the universal grippers need to squeeze the objects to wrap them around. This passive adaptive grasping way makes it difficult to grasp soft and smooth objects or grasp from a horizontal direction [21], [22].

For instance, if you try to grasp a balloon filled with water with a universal gripper, the balloon will deform under compression [see Fig. 1(a)]. A water cup placed on a table will slip when you try to grasp it horizontally with the universal gripper [see Fig. 1(b)]. All of these will cause grasp failure. On the contrary, the multifinger grippers with soft actuators perform better in

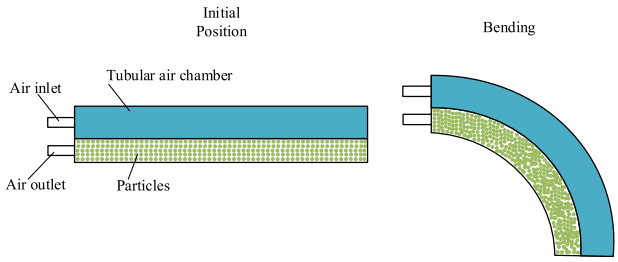

Fig. 2. "Sandwich" variable stiffness pneumatic soft actuator.

both cases because of their active adaptive grasping through bending deformation.

One of the typical soft actuators is a composite structure based on a pneumatic cavity and a particle cavity [21], [23], [24], [25], whose shape is similar to a sandwich [see Fig. 2]. The pneumatic cavity is responsible for the bending motion, the particle cavity containing particles can achieve the jamming effect. These grippers can adapt to objects with different shapes or sizes while achieving variable stiffness, demonstrating that particle jamming has excellent potential and research value in soft robotics. However, the volume of the particle cavity changes under different bend angles when the number of particles is constant, which is a challenge in determining the number of particles in the initial state. For instance, too many particles may weaken the restorability of the actuator and require a higher driving pressure. A small number of particles may lead to the unwanted contraction of the actuator during the vacuum suction.

Another type of particle jammed variable stiffness soft actuator is called particle transmission scheme [26], in which the particle volume fraction (the ratio of total particle volume to cavity volume) is dynamically adjusted according to the bend angle of the actuator. The grippers based on these actuators have a wide range of stiffness modulation. However, the jamming effect and gravity make it difficult for particles to flow out of the cavity, resulting in poor restorability of the actuators (see Fig. 3). For instance, the particles will concentrate at the bottom under the influence of gravity [27]. To solve this problem, Li et al. [23] proposed using vibration to promote the restorability of particles. Their research shows that vibration helps to improve the restorability of actuators, but the restoring effect is related to the contractility of the cavity. When the cavity contraction force is small, the restoring effect is limited. However, increasing the contraction force of the cavity will reduce the compliance of the actuator. Therefore, how to improve the restorability of particle transmission drivers is still a very important problem, but has not been solved.

Besides restorability, the compliance of a particle-driven actuator decreases during deformation because the bending and stiffness enhancement are both achieved by increasing the particle volume. For example, the stiffness of actuators increased by about six times and seven times in active deformation [12], [23]. Thus, the particle volume fraction has a significant impact on the actuator's performance, and the requirement of the volume fraction is different at different working stages. The particle volume fraction should be low during deformation to acquire better

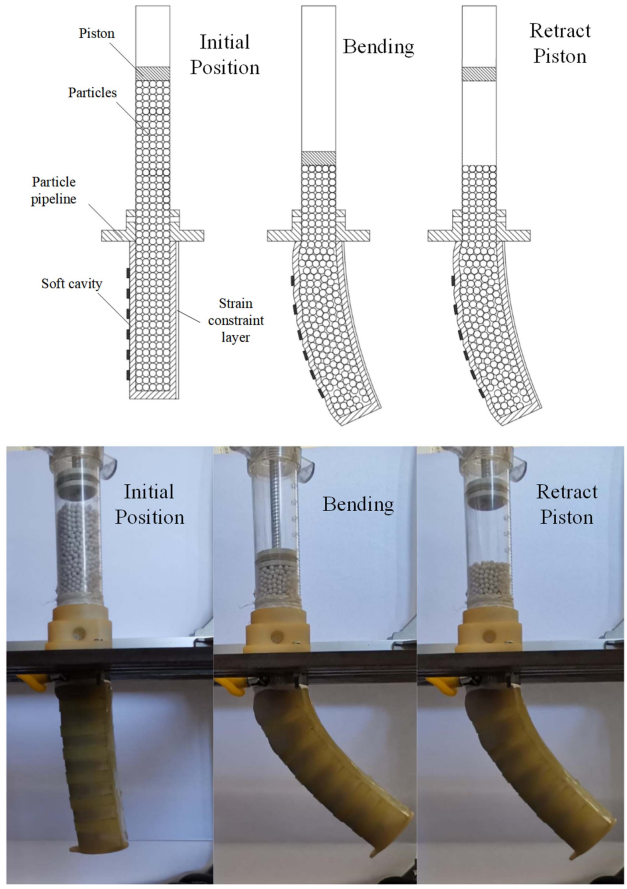

Fig. 3. Particle transmission soft actuator.

actuator compliance and high to get better stiffness enhancement. In order to obtain better variable stiffness performance, it is necessary to dynamically control the volume fraction of particulate matter at different stages of the driver.

In this article, we propose a new design of a variable stiffness soft actuator. We used strings of beads instead of discrete particles to improve the restorability of the actuator. To obtain variable stiffness performance, we combined the sandwich scheme with the particle transmission scheme. To reduce the loss of compliance during deformation, like the sandwich scheme, we used compressed air as the power source. To improve the stiffness modulation ability, like the particle transmission scheme, we dynamically increased the volume of the strings of beads in the actuator before vacuum suction.

The structure of this article is as follows: Actuator Design part introduces the structure and the parameter optimization of the actuator. Fabrication of Actuator part gives the fabrication methods of the actuator. Experiment of Actuator part shows the related performance of the actuator. Grasping Experiment and Discussion part shows the grasping performance of the gripper that consists of three proposed actuators.

II. Actuator Design

A. Design Goals and General Design Idea

Compliance and stiffness are contradictory attributes, so there are different requirements for ideal variable stiffness soft gripper

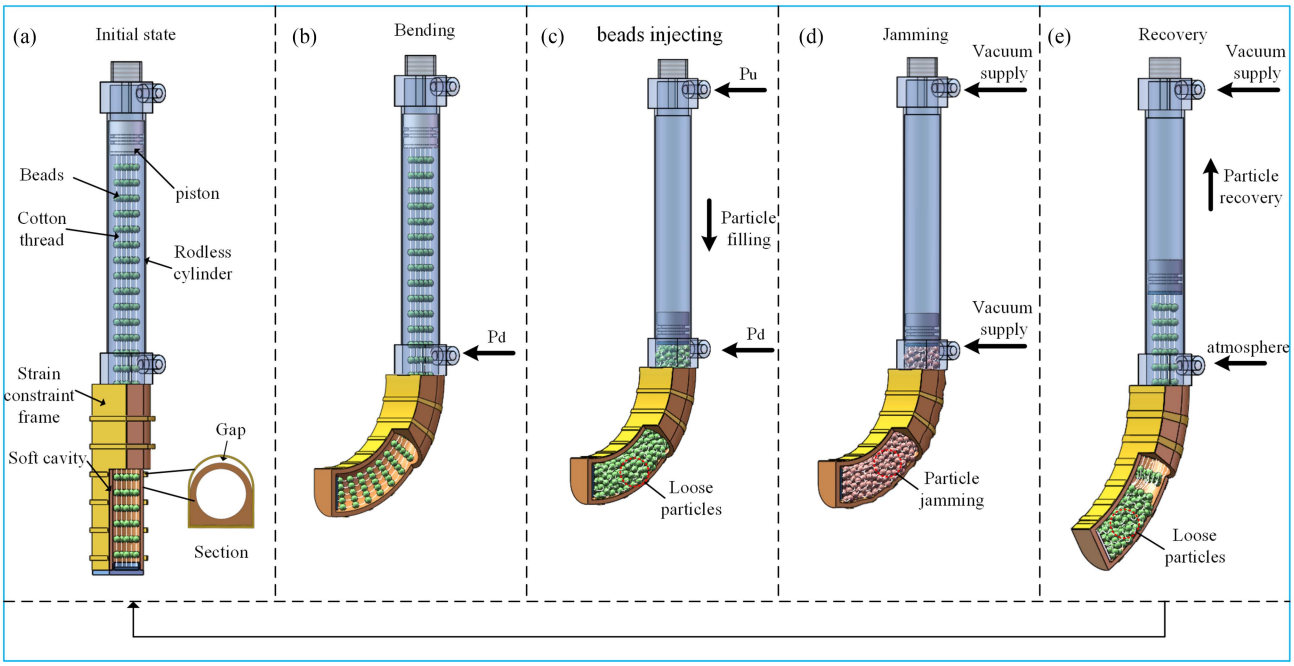

Fig. 4. Design concept of the actuator. (a) Structure of the actuator. (b) Bending deformation (c) beads injecting. (d) Particle jamming. (e) Particle recovery.

during different working stages. The gripper should be compliant when actively deforming to wrap the grasped object. When bearing the loads, the gripper should have high rigidity. To ensure the reliability of grasping, the gripper should also have an excellent shape-locking ability when stiffness-enhancing. To make the gripper work repeatedly, it should also have excellent restorability.

In this article, the variable stiffness soft gripper we design expects to have the following characteristics.

1) Excellent compliance during active deformation.
2) Large stiffness in the bearing stage.
3) Good shape-locking ability when the stiffness-enhancing.
4) Excellent restorability after an operation cycle.

Therefore, our overall design ideas are as follows (see Fig. 4).

1) In the active deformation stage, the actuator is driven by low-pressure gas to weaken the particle jamming effect, so as to improve the compliance of the actuator.
2) In the bearing stage, the stiffness of the actuator is improved by using the vacuum jamming effect of particles.
3) By controlling the particle volume fraction before and after the particle jamming, the actuator can reduce the volume shrinkage and obtains acceptable shape-locking ability.
4) By using strings of beads (see Fig. 6) instead of discrete particles, the restorability of the actuator can be significantly improved.

B. Design of Strings of Beads

A string of beads is made by combining some spherical particles with a flexible thread. The particles are fixed on the flexible thread with an equal interval (see Fig. 5). Ideally, when the strings of beads are pressed into the soft cavity, the pressure

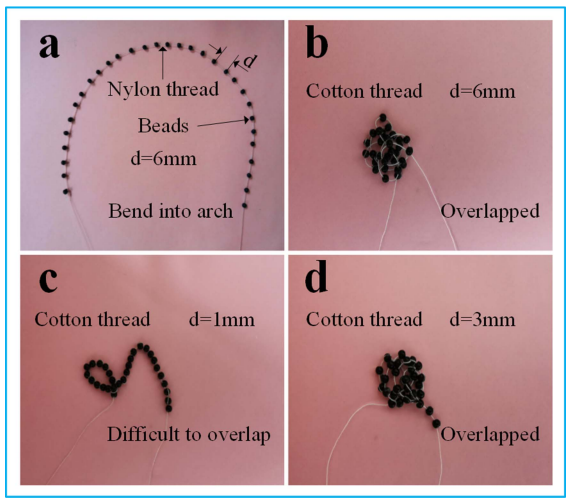

Fig. 5. Overlapping performance of the strings of beads with different threads and intervals d. (a) Nylon thread, $d = 6$ mm. (b) Cotton thread, $d = 6$ mm. (c) Cotton thread, $d = 1$ mm. (d) Cotton thread, $d = 3$ mm.

and friction between the particles dominate, and the flexible thread has little restriction on the particle movement. When the strings of beads need to be discharged from the soft cavity, the tension of the flexible thread is dominant, which can prevent particles from self-locking under pressure and friction.

1) Selection of Beads: The shape impacts the fluidity of beads and the bearing capacity under particle jamming. The particles with sharp angular shapes can be inlaid with each other to improve the bearing capacity. However, it will also lead to poor fluidity of beads, making it difficult to fill and flow into the soft cavity, so we selected spherical beads in this article.

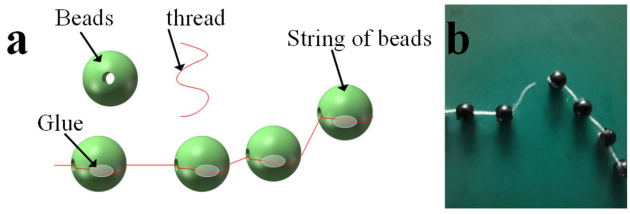

Fig. 6. (a) String of beads and its assembly method. (b) Reliability of the connection between beads and cotton threads.

Selecting a smaller beads diameter can increase the particle volume fraction, which is conducive to improving the bearing capacity. However, too-small beads will also lead to a too-small gap between beads, which is not beneficial to the formation of uniform vacuum distribution. At the same time, tiny beads will also increase the manufacturing difficulty of strings of beads, and we select the nominal size of 3mm beads($\bar{x}$= 2.957 mm, $\mu = 0.043$ mm).

The beads should be low-density. The density of glass, metal, and ceramic is too high, and its weight will affect the deformation of the actuator. Therefore, we select acrylic beads. In addition, the materials of beads should also have appropriate friction characteristics. Too large a friction coefficient makes it difficult for beads to fill the cavity, and too small a friction coefficient is not conducive to improving the bearing capacity of the actuator. The friction coefficient between acrylic and acrylic is too significant (close to 0.8), so a small amount of graphite powder is filled in the soft cavity as a solid lubricant to reduce the friction.

2) Selection of Flexible Threads: When selecting the flexible threads, the primary consideration is its bending resistance and blocking effect on particle movement. The flexible thread should have small bending resistance and sufficient tensile strength. In this article, we select two kinds of flexible threads that are readily available in the market: 402 cotton thread (QiaoLong 304 cotton thread) with a diameter of 0.16 mm and nylon thread(Handing 0.4# nylon thread) with a diameter of 0.104 mm. Although it is evident that the tensile strength of nylon thread with a diameter of 0.104 mm is greater than that of 402 cotton thread, the former has too large bending rigidity, which seriously hinders the movement of particles. We use the above two kinds of flexible thread to make a string of beads and slowly place the two strings of beads on the horizontal plane from the suspended state. It can be seen that nylon thread is challenging to overlap, and it may bend into an arch [see Fig. 5(a)]. This phenomenon means that the beads are hard to fill into the cavity. Conversely, the cotton thread is sufficiently soft [see Fig. 5(d)]. Therefore, we selected 402 cotton thread as the flexible thread material in this article.

3) Assembly Method of String of Beads: Fig. 5(a) shows the assembly method of beads and cotton thread, which can ensure the reliability of the connection between beads and cotton threads. A flexible cable passes through a hole in the middle of each particle, wraps around the particle, and then uses a binder to bond the two together. We used a tensile testing machine to break a string of beads and found that the connections between the beads and the cotton thread were strong enough even if the cotton thread was broken [see Fig. 6(b)].

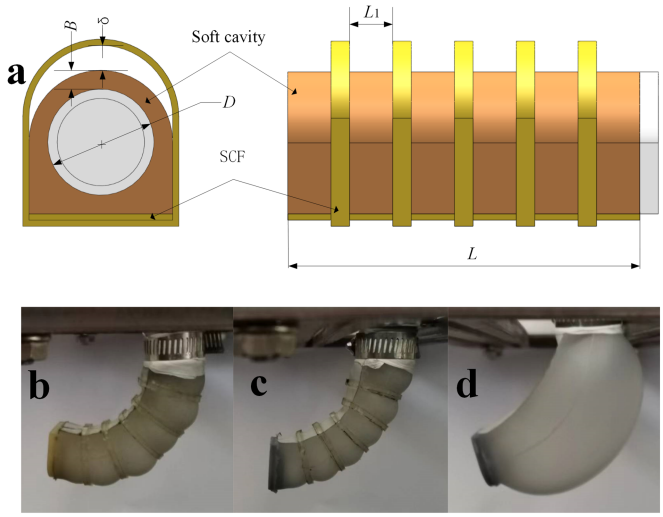

Fig. 7. (a) Structure of soft cavity with an initial noncontact strain constrain frame (INCSCF). (b) Soft cavity with an INCSCF (c) soft cavity with the strain constrain frame (SCF) directly bonded to the cavity. (d) Soft cavity without SCF.

The interval size (d) of beads should be appropriate. Intervals that are too small may hinder the dislocation between adjacent beads, and the string of beads will show similar properties to that of the nylon thread [see Fig. 5(c)]. Intervals that are too large enlarge the size of the actuator. The optimal bead interval was determined by reducing the interval from 6 to 1 mm. When the particle spacing was reduced to 3 mm, the overlapping state of the particle string did not change significantly.

Two factors should be considered when determining the length of the string of beads. The length should ensure that the particles can fill the deformed soft cavity and should be slightly longer than the overall length of the actuator to avoid the cotton thread blocking the active deformation of the cavity.

C. Design of Soft Cavity With an Initial Noncontact Strain Constrain Frame (INCSCF)

To ensure the compliance of the actuator in the active deformation stage, and to facilitate the strings of beads pressing in and pulling out, the soft cavity needs to have the following characteristics.

1) Large cross-section and smooth flow channel, so the common PneuNets structure is not suitable for our design.
2) Low required actuation pressure. Due to the hydrostatic skeleton effect, the greater the driving pressure, the lower the compliance of the actuator. The driving pressure of the fiber-reinforced soft cavity is as high as 70-150kPa, which is not suitable for our design.
3) Avoid the "balloon effect" caused by excessive local deformation of the cavity during inflation.

To meet the above three requirements at the same time, we proposed an INCSCF soft cavity structure (see Fig. 7). The inner part of the soft cavity is a silicone (Ecoflex 00-30) deformation chamber with a circular cross-section channel in the center. There is a constraint layer made of fabric (XiaoTaiYan shirting) at the bottom of the cavity, and the outer part is

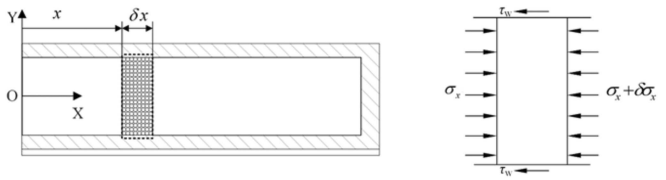

Fig. 8. Coordinate system of cavity force analysis and force analysis diagram of particle unit.

a strain constraint frame (SCF) with relatively high stiffness (polyurethane). The bottom of the cavity adheres to the SCF to limit its axial elongation. The gap between the cavity and the SCF enables the soft cavity to generate radial expansion to enlarge its cross-section size, which is beneficial to the flow of the particles. When the cavity expands and contacts the initial noncontact strain constrain frame (INSCF), the INSCF can limit the radial expansion of the soft cavity, thus inhibiting the balloon effect caused by the local expansion of the soft cavity [28]. Then, when the driving pressure increases, the bending deformation will become the main deformation movement.

When the bending angle of the driver with INCSCF reaches 90°, the driving pressure is about 12 kPa [see Fig. 7(b)], which is lower than 20 kPa when the SCF is directly bonded to the cavity [see Fig. 7(c)]. Without SCF, the soft cavity has a profound balloon effect in 8 kPa [see Fig. 7(d)].

The primary geometric parameters of the soft cavity design include diameter D of the internal flow passage, length L, the thickness B of the soft cavity, the gap δ between the cavity and the SCF, and the interval distance L_1 of the SCF [see Fig. 7(a)].

When D is too small, it is not easy to smoothly press or pull the strings of beads into or out of the soft cavity. At the same time, more particles in the same section will lead to lower ultimate bearing capacity and poor restorability of the actuator. If D is too large, the vacuum pressure is challenging to reach the center of the driver effectively, making some particles not fully play their role. We make $D = 17$ mm in the existing design.

Due to the influence of friction, when particles are pressed into the slender channel, the pressure transmitted between particles near the inlet is significant. In contrast, the force transmitted between particles far away from the inlet is small. In this article, we use the differential slice method based on the Janssen model to establish the distribution model of σ_{x}, which is the longitudinal pressure between particles when pressed into the cylindrical channel (see Fig. 8). We can obtain the following equations from the balance of the unit in the X direction:

$$\begin{cases} \tau_{\mathrm{w}} = \mu_{\mathrm{w}}\sigma_{\mathrm{y}} \\ \sigma_{\mathrm{y}} = K_{\mathrm{A}}\sigma_{\mathrm{x}} \\ (\pi D^2/4)(\sigma_{\mathrm{x}} + \delta\sigma_{\mathrm{x}}) + \pi D\delta\sigma_{\mathrm{x}}\tau_{\mathrm{w}} = \sigma_{\mathrm{x}}(\pi D^2/4) \end{cases} \tag{1}$$

where μ_{w} is the friction coefficient between particles and cavity; K_{A} is Janssen constant, and it can be calculated by the following equation:

$$K_{\mathrm{A}} = \frac{1 - \sin\phi}{1 + \sin\phi} \tag{2}$$

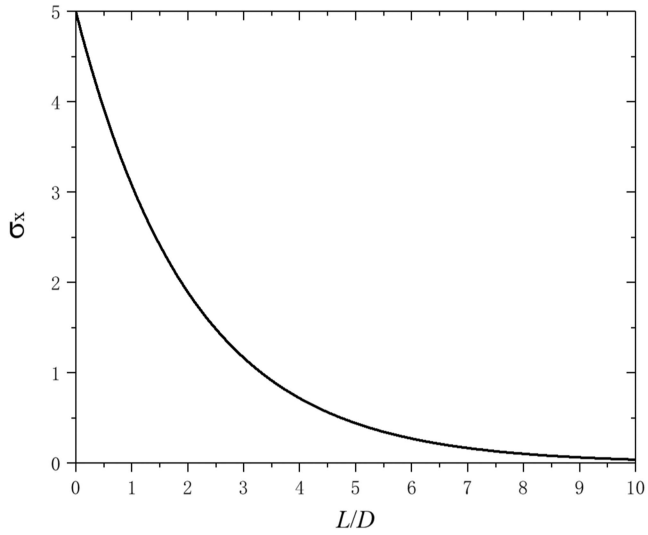

Fig. 9. Relationship between σ_{x} and $\frac{L}{D}$.

where ϕ is the internal friction angle of particles

$$\sigma_{\mathrm{x}} = C\exp\left(\frac{-4\mu_{\mathrm{w}}K_{\mathrm{A}}x}{D}\right) \tag{3}$$

where C is the distributed pressure on particles from the piston.

Taking the typical values of $\mu_{\mathrm{w}} = 0.364$, $\phi = 30°$, $C = 5$ kPa, the relationship between σ_{x} and the dimensionless parameter $\frac{L}{D}$ was caculated through (3) and the results is shown as Fig. 9. It can be seen that the conduction of particle pressure decreases exponentially with the increase in channel length, and when $\frac{L}{D}$ is greater than 3.5, it is close to 0, which means that when $\frac{L}{D}$ is too large, it is difficult to transmit the piston thrust to the bottom of the cavity, so we make $L = 60$ mm (about 3.5 times D).

To explore the influence of B, δ, and L_1 on the driving pressure and bending angle of the soft cavity. We used Abaqus 2018 (Simulia; Dassault Systems) to carry out a series of FEA calculations to obtain a better combination of design parameters (see Fig. 10). Through the uniaxial tensile test, we have obtained the hyperelastic constitutive models of Ecoflex 00-30, polyurethane and the fabric (see Table I).

It can be seen from Fig. 10 that when $B = 2$ mm, the bending angle is large, reaching 126°, but a profound balloon effect is produced, which is unfavorable for the strength of the soft cavity and the filling of particles. When $B = 4$ mm, the bending angle of the soft cavity is only 36°, which cannot meet the functional requirements; Therefore, we make $B = 3$ mm.

The smaller the L_1 is, the larger the bending angle of the soft cavity is; the values are 94°, 84°, and 78°, respectively, and the change is not apparent. When $L_1 = 10$ mm, the constraint frame cannot well limit the balloon effect of the soft cavity. When L_1 is reduced, although the bending angle of the cavity will be reduced, the balloon effect will be significantly reduced because the increase in the number of constraint rings will make the soft cavity expand more evenly. Therefore, in this article, we make

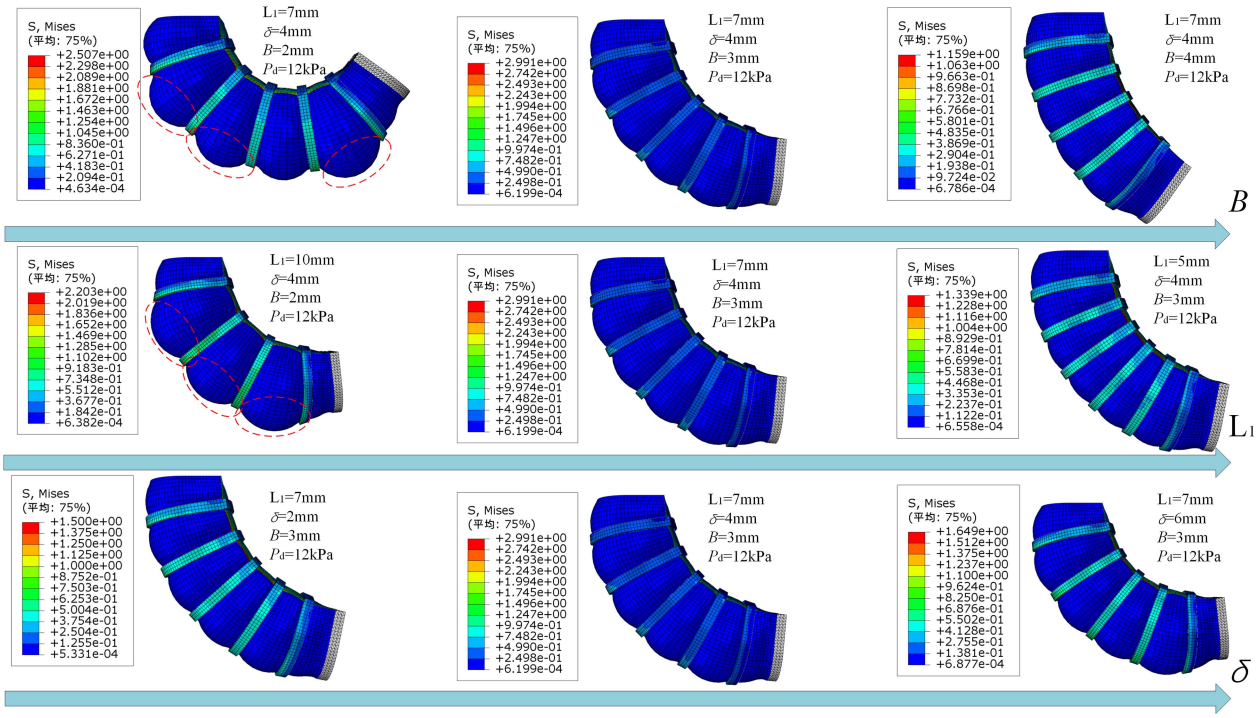

Fig. 10. Finite element simulation of actuator bending angle with different parameter combinations.

TABLE I
MATERIAL MECHANICS MODEL

Material	Ecoflex 00-30	Polyurethane	Fabric
Material model	Ogden ($\mu_1 = -0.3128$MPa, $\mu_2 = 0.19$ MPa, $\mu_3 = 0.145$ MPa, $\alpha_1 = 2.082$, $\alpha_2 = 2.506$, $\alpha_1 = 1.49$,),	Mooney-Rivlin($C_{01} = 0.257$ MPa, $C_{10} = 2.206$ MPa)	Linear elastic($E_j = 0.27$MPa, $E_w = 0.54$MPa, $V_{12} = 0.2$, $G = 0.02$MPa,)

$L_1 = 7$ to enable the actuator to obtain a larger bending angle without a noticeable balloon effect.

The larger the δ, the larger the deformation angle of the cavity. The values are 77°, 84°, and 94°. However, when δ increases, the internal volume of the soft cavity becomes more extensive, which means that more particles are needed to fill the soft cavity. However, the increase in the number of strings of beads will lead to the overall size of the actuator becoming more significant and the manufacturing difficulty increasing. Therefore, we can make $\delta = 4$ mm to ensure a large bending angle when limiting the number of particles.

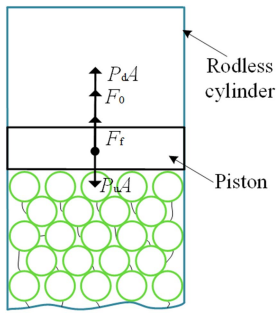

Fig. 11. Piston force diagram.

D. Force Analysis of Piston

The piston force diagram is shown in Fig. 11. Neglecting the gravity of the piston, we obtained the following equations:

$$P_u A = F_0 + P_d A + F_f \tag{4}$$

where P_d is the driving pressure in the soft cavity, A is the area of the piston bottom, and F_f is the friction force on the piston from the wall, depending on how the piston moves, the friction force can be either sliding friction or static friction. For simplicity, the amplitude of sliding friction is constant and equal to the amplitude of the maximum static friction force. The force of friction is defined as positive when it is up.

The pressure difference between the two sides of the piston will determine the state of motion of the piston. When $(P_u - P_d)A > F_0 + F_f$, the piston moves downward; when $(P_u - P_d)A < -F_f$, the piston moves up; at $-F_f < (P_u - P_d)A < F_0 + F_f$, the piston remains stationary. The higher contact force F_0 between the piston and the beads means the beads have a higher particle volume fraction. We adjust F_0 by changing P_u(the pressure in the upper cavity of the rodless

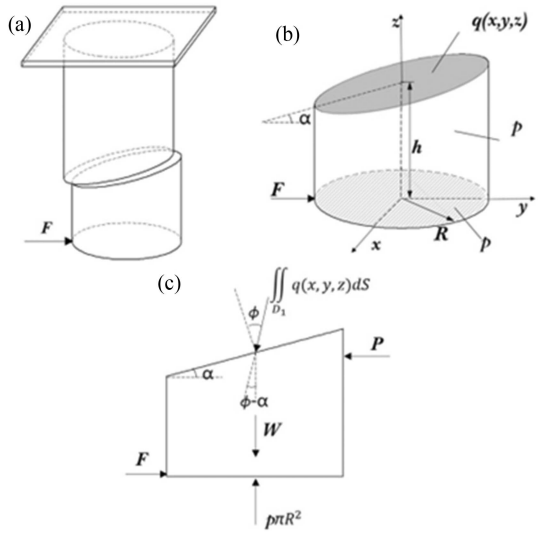

Fig. 12. (a) Formation of separation body. (b) Parameters of the separation body. (c) Force analysis diagram of the separated body.

cylinder).When the P_u reaches the corresponding value, we consider the particle volume fraction meets the requirement.

E. Establishment of Actuator's Stiffness Model

In order to predict the bearing capacity of the actuator, it is necessary to establish the stiffness model. In this article, we use the limit equilibrium method to analyze the force of particles in the cavity. We made the following assumptions.

1) Particle matter is assumed to be non-viscous molar-Coulomb material;
2) The failure slip surface is a plane;
3) Ignoring the elastic restoring force of the soft cavity and the friction force on the particles.

We take the actuator without bending deformation as the research object. Its internal particles are jammed to form a cylindrical cantilever beam [see Fig. 12(a)]. Its upper end is fixed, and its lower end is subjected to horizontal external force F. Under the action of F, particles in the cavity will slip on the sliding surface, the height of the sliding surface is h, and the included angle with the horizontal plane is α. Taking part below the imaginary sliding surface of the actuator as the separation body [see Fig. 12(b)], it tends to slip to the right. The load borne by the separation body includes the following.

1) Negative pressure uniformly distributed load p acting on the side wall and bottom surface;
2) Horizontal external load F acting on the bottom;
3) Material weight W;
4) Internal binding force $q(x, y, z)$ acting on the imaginary sliding surface, and according to Mohr-Coulomb law, under the limit state, the included angle between the direction of $q(x, y, z)$ and the normal direction of the imaginary sliding surface is the internal friction angle of particles ϕ.

For the separated body, the equilibrium equations of force in horizontal and vertical directions are written.

Vertical force equilibrium equation:

$$p\pi R^2 - W = \iint_{D_1} q(\mathrm{x},\mathrm{y},\mathrm{z})\mathrm{d}S \cdot \cos(\phi-\alpha),$$

$$D_1 : \left\{ (\mathrm{x},\mathrm{y}) \middle| x^2 + y^2 \le R^2 \right\}. \tag{5}$$

Horizontal force equilibrium equation:

$$F - P = \iint_{D_2} q(\mathrm{x},\mathrm{y},\mathrm{z})\mathrm{d}S \cdot \sin(\phi-\alpha) \tag{6}$$

$$P = \iint_{D_2} p\frac{\sqrt{R^2-x^2}}{R}\mathrm{d}A = p\pi R^2 \tan\alpha,$$

$$D_2 : \left\{ (\mathrm{x},\mathrm{y}) \middle| x^2 + \left(\frac{z-h}{\tan\alpha}\right)^2 \le R^2 \right\} \tag{7}$$

where material weight $W = \pi R^2 h\gamma$, and γ is the weight density; R is the radius of the cavity; P represents the effect on the y-axis direction of the separation body under the negative pressure uniform load p on the side wall; ϕ is the internal friction angle of particulate matter dS is a small area on the imaginary sliding surface; dA is the small curved surface area of the side wall of the separation body.

Combining (5) and (6), we can obtain the following equation:

$$F(h,\phi) = p\pi R^2 \tan\alpha + \pi R^2(p - h\gamma)tan(\phi-\alpha). \tag{8}$$

The maximum load the driver can bear corresponds to the minimum value of (8) $F_{\min}(h,\phi)$.

Taking $\gamma = 7546$ N/m^3, $R = 8.5$ mm, $p = 80$ kPa, $\phi = 30°$, we calculated the maximum carrying capacity of the driver as 7.9 N, the corresponding height of the slip plane $h = 58$, and the included angle of the slip plane $\alpha = 14.7°$.

III. Fabrication of Actuator

1) *String of beads fabrication:* We used cotton threads to string beads together. To ensure the reliability of the connections between cotton threads and particles, we placed a little glue (Valigoo silicone special glue) on the bead surface [see Fig. 13(a)]. Then, the string of beads was attached to the thread boards on the piston and cap [see Fig. 13(b)].
2) *Soft cavity fabrication:* The soft cavity was cast by a three-dimensional (3-D) printed mold, and its inner and outer surfaces were formed by the inner and outer molds [see Fig. 13(c)], respectively. Then, the SCF, consisting of a constraint layer and several constraint rings, was bonded to the soft cavity [see Fig. 13(d) and (e)] (Valigoo silicone special glue).
3) *Assembly:* The soft cavity was attached to the rodless cylinder (AirTAC RMS20) by a pipe hoop. Then, the piston entered the rodless cylinder from the bottom of the soft cavity and the cap for sealing was glued to the cavity [see Fig. 13(f)] (Valigoo silicone special glue). The actuator was connected to the pneumatic system by the air tubes to control the driving pressure.

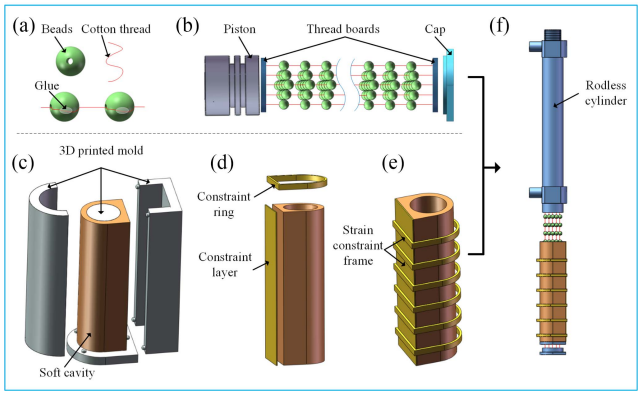

Fig. 13. Fabrication of the actuator. (a) Stringing the beads. (b) Attaching the strings of beads to the piston and cap. (c) Molding the soft cavity. (d) Attaching the constraint layer and constraint rings to the soft cavity. (e) Soft cavity with SCF. (f) Assembly.

IV. Experiment of Actuator

To assess the performance of the proposed design, we tested the restorability, variable stiffness ability, and compliance of the prototype actuator through a series of experiments. The test device [see Fig. 14(a)] was composed of an actuator, horizontal linear modules, a force gauge, and a pressure control system. The horizontal module drives the force gauge to measure the force of the actuator against the gauge, pressure control system adjusts the input pressure P_{u} and P_{d}.

Before testing the performance of the actuator, it is necessary to determine the proper values of the driving pressure P_{d} and P_{u}.

To determine the value of P_{d}, we first recorded actuator bending angles at different pressure P_{d} [see Fig. 14(b)]. It is found that when the driving pressure was less than 8 kPa, the actuator had no obvious bending deformation, and the soft cavity had not yet contacted the restraint frame. As the pressure increased further, the bending angle increased gradually. When the pressure reached 12 kPa, the actuator bent to 80°, which is sufficient for grasping. Therefore, in subsequent experiments, the value of P_{d} was set at 12 kPa. At the same time, we compared and tested the deformation ability of the actuator when there was no gap between the restraint frame and the silicone cavity, and found that the actuator needed 20 kPa driving pressure to reach a bending angle of 83° [see Fig. 14(b)]. This illustrates the obvious benefits of INSCF for reducing drive pressure.

According to the force analysis of the piston, increasing P_{u} will increase the pressure of piston on particles in the stage of particle pressing. If P_{u} is too small, the filling will be too loose, resulting in additional deformation during internal vacuum pumping to force particles jamming, which is not conducive to shape-locking. If the P_{u} is too large, the cavity will be further expanded and the compliance of the driver will be reduced. For optimal shape-locking, the appropriate P_{u} value should be as large as possible without causing undesired deformation of the actuator. It was found that when $P_{\mathrm{d}} = 20$ kPa and $P_{\mathrm{u}} > 53$ kPa, the actuator would have significant expansion (especially near the inlet of the flow channel). So, the value of P_{u} in the following experiments was 53 kPa.

A. Restorability

Restoring the actuator to the initial state after completing a grasping action is a pivotal requirement for the use of a soft gripper. With better restorability, the gripper can work repeatedly, and the grasping performance in each cycle will be consistent.

In this test, we made a mark on the cap and the restorability was represented by the distance ΔS between the mark positions before deformation and after recovery [see Fig. 14(c)]. To facilitate the comparison with actuators of different sizes, the ΔS was normalized by the length l of the actuator (72 mm). The ΔS of the actuator with discrete particles was also measured by the same method. The mark position was recorded by a camera and computed by image processing. At each pressure P_{d}, we tested five times, and ΔS was the average value of the five data.

The results are shown in Fig. 13(c), from where we can see that the ΔS of the actuator with discrete particles is higher than that with strings of beads. For example, when P_{d} is equal to 8 kPa and 12 kPa, the ΔS_1 is 12.7% and 36.7% of the l, which are more than thirty and twelve times larger than ΔS_2 (0.4% and 2.9% of the l), respectively. The average value of ΔS_1 (23.62% of the l) is more than sixteen times than ΔS_2 (1.44% of the l). The good performance is attributed to the strings of beads that can pull the beads back to their initial positions. In addition, the maximum value of ΔS_2 (2.9% of the l) occurs when $P_{\mathrm{d}} = 12$ kPa. The reason may be that the tiny slippage between the cavity and the particle pipeline increased with P_{d}.

B. Compliance and Variable Stiffness

Compliance refers to the degree of difficulty for an elastomer to deform under the action of external forces, which is the opposite of stiffness. High compliance means low stiffness and vice versa. Experiments were carried out to test the compliance of the actuator at the active deformation stage and the stiffness after rigidization. In the experiments, the driver was forced to produce 10 mm displacement, and the output force F generated by the driver is used as the characterization parameter of compliance and stiffness [see Fig. 14(d)]. In the active deformation stage, the minor F, the better the compliance. In the bearing stage, the more significant F, the stronger the actuator's stiffness. The F of the proposed actuator during active deformation and stiffness modulation are recorded as F_{a1} and F_{s1}, respectively. The F of the actuator with discrete particles are recorded as F_{a2} and F_{s2}, respectively, The F of the pneumatic actuators without particles is recorded as F_{p}.

First, we arranged for the force gauge to contact the end cap when the actuator bent at pressure P_{d}. Then, the horizontal module was turned ON, and the force gauge pushed the actuator forward 10 mm. The reading of the force gauge is recorded as F_{a1} when the module stopped. Then, the actuator was returned to its initial state. The same P_{d} was supplied again. When the particle filling was finished, a vacuum pressure of -80 kPa was supplied. The reading of the force gauge is recorded as F_{s1} when the actuator was pushed forward 10 mm.

The relationships of the F versus P_{d} are shown in Fig. 14(d). The average value of force F_{a2} under different pressures is 2.63 N, which is more than five times larger than F_{a1} (0.47 N).

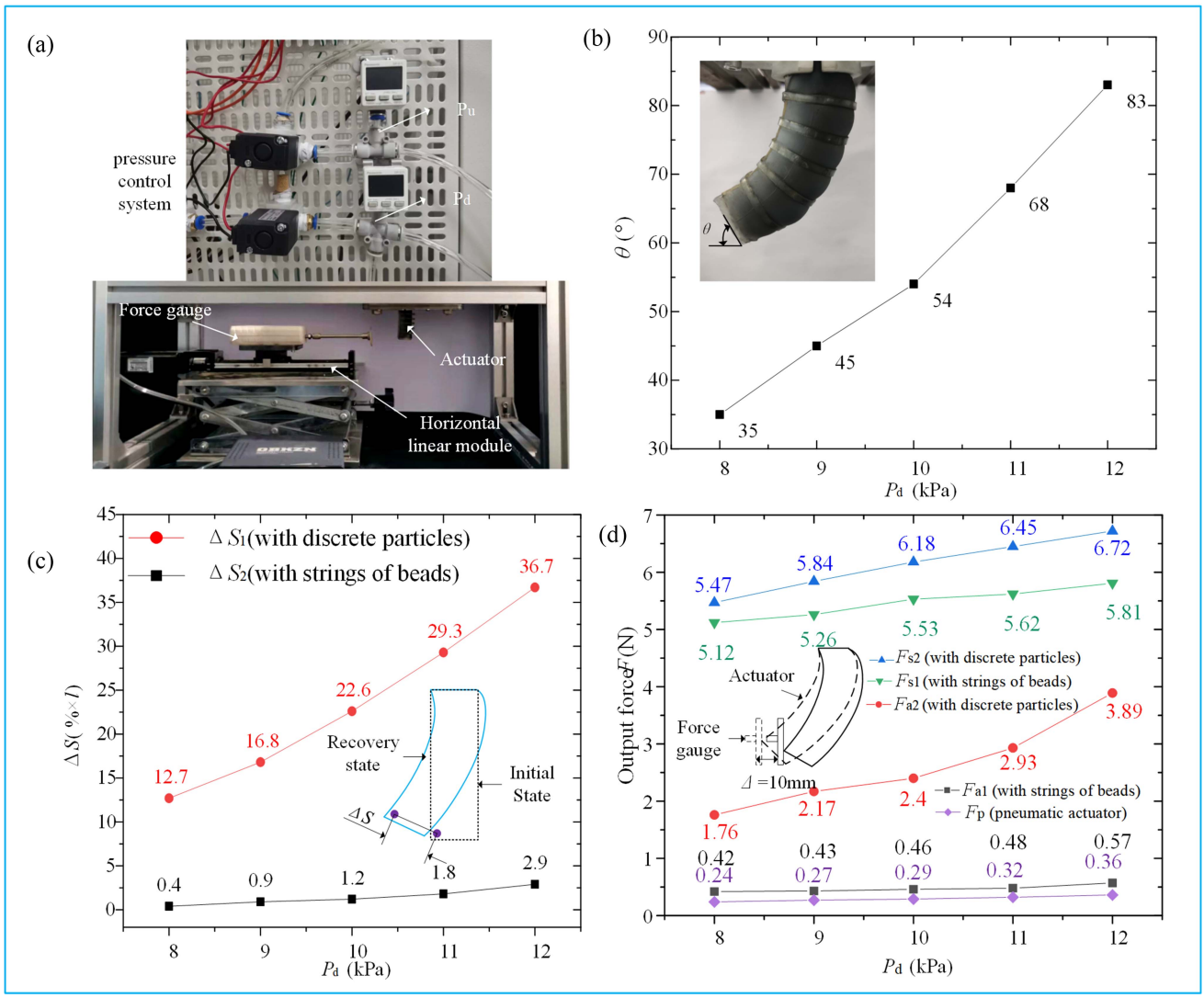

Fig. 14. Experimental setup and the results. (a) Performance test device of the actuator. (b) Definition of θ and the relationship of θ versus P_{d}. (c) Definition of ΔS and the values of ΔS at different P_{d}. (d) Definition of the output force F, and the results of the compliance and variable stiffness.

It indicates that the proposed actuator is more flexible than the actuator with discrete particles, and F_{a1} is close to F_{p}, which means the actuator has compliance close to pneumatic actuators. Because during active deformation, compressed air is the power source, and the particles have not filled the cavity at this time, the impact on the external force of the cavity is small.

The actuator can fleetingly stiffen under vacuum pressure, and the average value of the force F_{s1} reaches 5.47 N, which is nearly twelve times larger than F_{a1}. Besides, the average value of the force F_{s2} is 6.13 N, which is only about 1.12 times larger than F_{s1}. So, the proposed actuator has better compliance and similar bearing capacity compared with the actuator with discrete particles. It is worth noting that the experimental value (5.81 N) of the maximum carrying capacity is smaller than the theoretical value (7.9 N). The possible reason is that the particles are regarded as uniform medium in the theoretical modeling, and the nonuniformity of distribution is not considered. However, the actual plastic flow of particles always occurs in the local loose part.

V. Design of Gripper and Functioning Stages

A. Structure of Soft Gripper

The soft gripper (see Fig. 15) comprises three flexible soft fingers, each of which is an independent bending actuator. In addition to the deformable soft cavity and INCSCF, each actuator includes a rigid aluminum alloy rodless cylinder and a piston that can move in the barrel. Three actuators were fixed on a stationary platform.

The piston divides the rodless cylinder into the upper and lower chambers. The upper chamber end seal can be connected with compressed air or negative suction pressure under the control of reversing valve V1 (see Fig. 16); the lower chamber is connected with the flow channel of the soft deformation chamber and can be connected with compressed air, vacuum or atmosphere, respectively under the combined control of the reversing valve V2 and V3. The strings of beads are installed in the lower chamber, and the upper end of the beads is consolidated

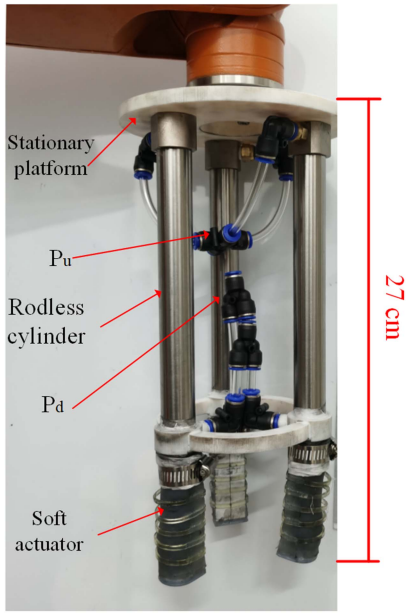

Fig. 15. Structure of the soft gripper.

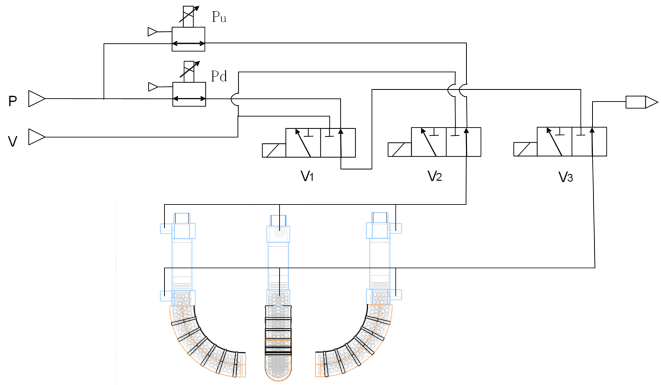

Fig. 16. Pressure control system.

with the piston. In order to prevent the beads from winding and knotting, the lower end of the beads is consolidated at the end of the deformable soft cavity.

B. Functional Stages of Soft Gripper

There are four functional stages of soft gripper.

1) *Active deformation stage:* The status of V1 is OFF, and the other valves are ON. The upper chamber is negative pressure, while the lower chamber is positive pressure P_{d}, which controls the final bending degree that the actuator can achieve.
2) *Beads injecting stage:* The status of V3 is ON, and the other valves are OFF. The upper and lower chambers are positive pressure, and $P_{\mathrm{u}} > P_{\mathrm{d}}$. At this time, $(P_{\mathrm{u}} - P_{\mathrm{d}})A > F_0 + F_{\mathrm{f}}$, and the beads are pressed into the soft cavity. F_0 can reflect the volume fraction of the particles. When F_0 is too large, the actuator's compliance will be reduced, while the shape-locking ability in the stiffness strengthening process will be insufficient when F_0 is too small.
3) *Load bearing stage:* The status of V2 is OFF, and the other valves are ON. Both the upper and lower chambers are negative pressure, and the strings of beads have particle jamming under the action of external atmospheric pressure. At this time, the driver has a strong bearing capacity.
4) *Particle recovery stage:* When the status of V2 is ON, the lower chamber is connected to the atmosphere. The state of V1 does not affect the lower chamber. V3 is OFF, the upper chamber is negative pressure, the atmospheric pressure can press the piston back to its original position, and the string beads are pulled out of the deformation chamber. The actuator is recovers to its initial state.

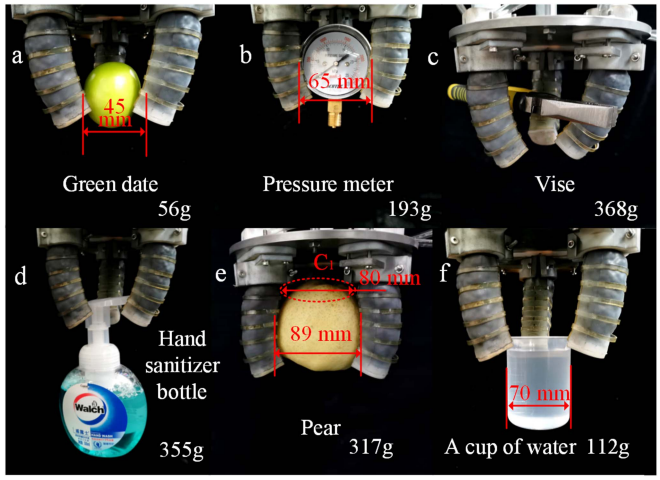

Fig. 17. Grasping different objects such as (a) a green date, (b) pressure meter, (c) vise, (d) hand sanitizer bottle, (e) Pear, and (f) cup of water.

VI. Grasping Experiment and Discussion

A. Shape Adaptability

To evaluate the shape adaptability of the gripper, we used the gripper to grasp several commonly used objects. Successful grasping is defined as the ability to grasp five times in a row and hold steady for five seconds.

Results are shown in Fig. 17. First, we can see that the maximum size that can be successfully is 89 mm, while the diameter of circle C_1 tangent to the constraint layers is 80 mm [see Fig. 17(e)], which means that the gripper can grasp larger ball-type objects. Second, the gripper can grasp objects of various shapes, such as a green date [see Fig. 17(a)], a pressure meter [see Fig. 17(b)], a vise [see Fig. 17(c)], a hand sanitizer bottle [see Fig. 17(d)], and a and a cup of water [see Fig. 17(f)].

B. Material Adaptability

The gripper can grasp soft and smooth objects such as a balloon full of water [see Fig. 18(a) and Supplementary Video], and a piece of tofu [see Fig. 18(b) and Supplementary Video], indicating good adaptability of the gripper to the hardness of the object.

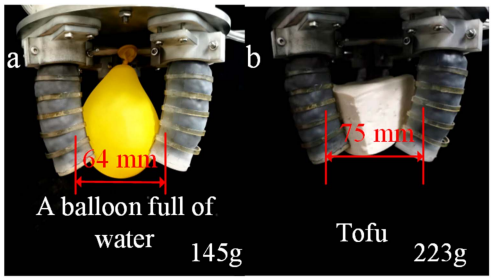

Fig. 18. Grasping soft and smooth objects such as (a) a balloon of water and (b) a piece of tofu.

C. Grasping Direction Adaptability

Grasping direction reliability refers to whether the grasping can remain reliable when the gripper position change. Thus, we conducted two experiments: 1) grasping objects in different directions [see Fig. 19(a)–(d)], and 2) grasping objects when there is an eccentric distance e between the gripper's axis and the object's axis [see Fig. 19(e)–(g)].

In the first experiment, the gripper has the preferable performance to the universal gripper in lateral grab [see Fig. 19(a)–(d)]. For example, when α is equal to 30° and 90°, the gripper can successfully grasp a cucumber and a 3-D printed ball, respectively. The experimental results show that the active adaption enables the gripper to grasp different objects from different directions without harming the objects' surface and indicate good reliability and versatility of the gripper.

In the second experiment, the target objects were two 3-D printed molds with a radius of 30 mm. One mold could slide on the table while the other could not. The objects were placed in contact with an actuator. So, the e is equal to 10 mm, which is a quarter of the radius of circle C_1. We can see that whether the objects can move or not, the grasping actions are both successful [see Fig. 19(f)]. Thus, the gripper has good adaptability against the changing of the gripper position because 10 mm is a large value for mechanical positioning accuracy.

D. Bearing Test

To test the maximum weight that can be stably grasped, we continuously added weights to the 3-D printing mold, and the results (see Fig. 20) showed that the gripper could grasp 2.744 kg of weight at the most.

E. Lifting Efficiency

In this work, the lifting efficiency is assessed by the time (t) it takes to complete a grasping action. Particle filling and recovery, the two most time-consuming processes, were realized by the piston movement. Due to the pneumatic drive, the piston movement speed is fast, the actuator bending and particle filling takes about 1 s, the vacuum suction takes about 0.5 s, and the particle recovery stage also takes about 1 s (Supplementary Video). The gripper has high lifting efficiency.

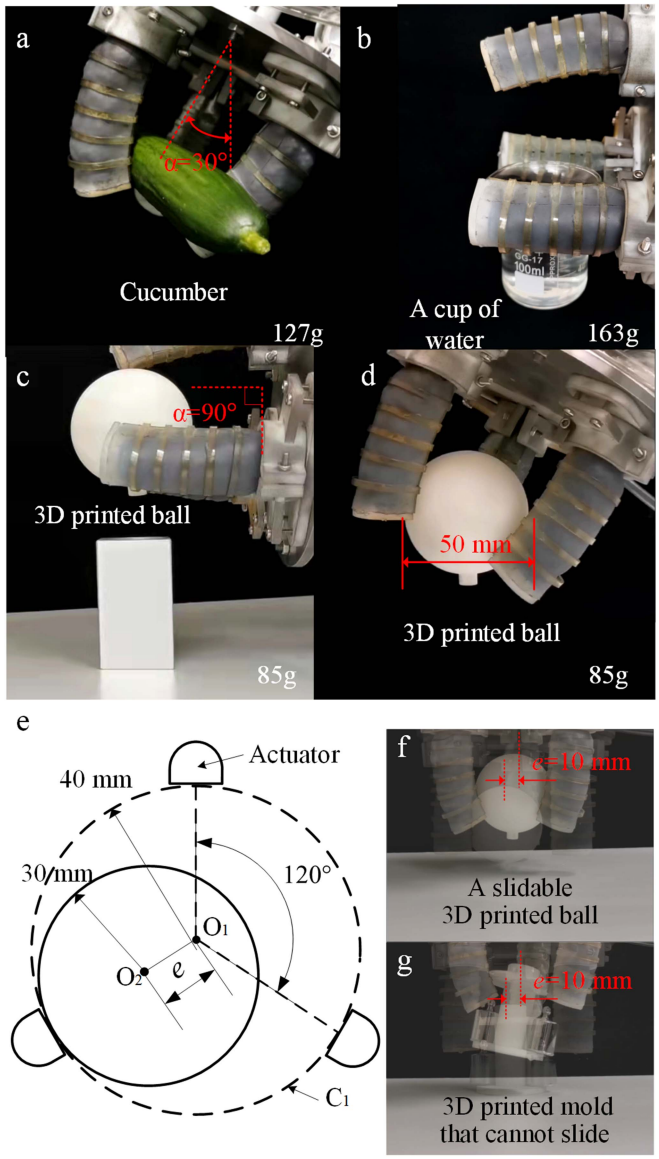

Fig. 19. Grasping different objects from different directions. (a) Cucumber laterally, and (b) a cup of water when α is 90°. (c) Three-dimensional-print ball, and (d) a 3-D-print ball when the α is 30° or grasping. (e) Diagram of eccentric grasp. (f) Grasping a slidable 3-D-print ball when e is 10 mm. (g) Grasping a 3-D-print mold that cannot slide.

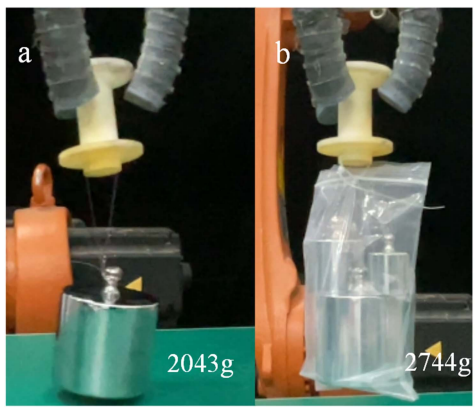

Fig. 20. Grasping maximum weight test. (a) 2043 g. (b) 2744 g.

VII. Conclusion

We have developed a novel soft robotic gripper with excellent restorability, compliance, and stiffness modulation ability. We innovatively connected the beads with cotton threads to form strings of beads, which, by pulling the cotton thread, improved the restorability of the actuator. In addition, we designed a novel INCSCF for the actuator. In the natural state, the soft cavity is not in full contact with the INCSCF, and the soft cavity can expand under air pressure to facilitate the flow of the string of beads. When the pressure increases, the INCSCF can inhibit the local balloon effect of the soft cavity. As for the control strategy, we used compressed air as the power source to drive the actuator. The string of beads is used to fill the soft cavity. The volume fraction of the beads in the soft cavity is reflected by the contact force between the beads and the piston.

The experimental data showed that the actuator was flexible and compliant during bending and rapidly stiffened under particle jamming. The beads could be restored to the initial position by pulling the threads, and the actuator had good restorability. The air pressure of the actuator with INCSCF was about three-fifths that of the actuator without INCSCF. The soft gripper based on the actuator has good performance in terms of reliability, adaptability, universality, and bearing capacity. Therefore, we expected that our proposed soft gripper will have broad application.

To further improve the performance of the gripper, some parameters, such as the diameter of the beads and the layout of the stings of beads, require optimization through additional experiments and theoretical analysis. Besides, our idea can also be applied to other scenarios, such as twist soft actuators and walking robots. These researches will be put on the agenda in our ongoing work, and an improved gripper may be developed in the future.

References

[1] C. Laschi, B. Mazzolai, and M. Cianchetti, "Soft robotics: Technologies and systems pushing the boundaries of robot abilities," *Sci. Robot.*, vol. 1, no. 1, 2016, Art. no. eaah3690.

[2] C. T. Kiang, A. Spowage, and C. K. Yoong, "Review of control and sensor system of flexible manipulator," *J. Intell. Robot. Syst.*, vol. 77, no. 1, pp. 187–213, Jan. 2015.

[3] M. Manti, V. Cacucciolo, and M. Cianchetti, "Stiffening in soft robotics: A review of the state of the art," *IEEE Robot. Autom. Mag.*, vol. 23, no. 3, pp. 93–106, Sep. 2016.

[4] Y. Fei, J. Wang, and W. Pang, "A novel fabric-based versatile and stiffness-tunable soft gripper integrating soft pneumatic fingers and wrist," *Soft Robot.*, vol. 6, pp. 1–20, 2018.

[5] Y. Haibin, K. Cheng, L. Junfeng, and Y. Guilin, "Modeling of grasping force for a soft robotic gripper with variable stiffness," *Mechanism Mach. Theory*, vol. 128, pp. 254–274, 2018.

[6] S. Yoshida, Y. Morimoto, L. Zheng, H. Onoe, and S. Takeuchi, "Multipoint bending and shape retention of a pneumatic bending actuator by a variable stiffness endoskeleton," *Soft Robot.*, vol. 5, pp. 718–725, 2018.

[7] C. Majidi and R. J. Wood, "Tunable elastic stiffness with microconfined magnetorheological domains at low magnetic field," *Appl. Phys. Lett.*, vol. 97, 2010, Art. no. 164104.

[8] Y.-J. Kim, S. Cheng, S. Kim, and K. Iagnemma, "A novel layer jamming mechanism with tunable stiffness capability for minimally invasive surgery," *IEEE Trans. Robot.*, vol. 29, no. 4, pp. 1031–1042, Aug. 2013.

[9] V. Wall, R. Deimel, and O. Brock, "Selective stiffening of soft actuators based on jamming," in *Proc. IEEE/Int. Conf. Robot. Autom.*, 2015, pp. 252–257.

[10] X. Zeng and H. Su, "A high performance pneumatically actuated soft gripper based on layer jamming," *Amer. Soc. Mech. Eng. J. Mechanisms Robot.*, vol. 15, no. 1, Feb. 2023, Art. no. 014501, doi: 10.1115/1.4053857.

[11] Y. Wei, Y. Chen, Y. Yang, and Y. Li, "A soft robotic spine with tunable stiffness based on integrated ball joint and particle jamming," *Mechatronics*, vol. 33, pp. 84–82, 2016.

[12] Y. Li, Y. Chen, Y. Yang, and Y. Wei, "Passive particle jamming and its stiffening of soft robotic grippers," *IEEE Trans. Robot.*, vol. 33, no. 2, pp. 446–455, Apr. 2017.

[13] A. Cavallo, M. Brancadoro, S. Tognarelli, and A. Menciassi, "Granular jamming based robotic gripper for heavy objects," *Proc. Estonian Acad. Sci.*, vol. 6, no. 2, pp. 161–173, 2019.

[14] J. Miettinen, P. Frilund, I. V. Aida, P. Kuosmanen, and P. Kiviluoma, "A soft retraction system for surgery based on ferromagnetic materials and granular jamming," *Soft Robot.*, vol. 68, no. 4, pp. 421–428, 2019.

[15] L. Al Abeach et al., "A variable stiffness soft gripper using granular jamming and biologically inspired pneumatic muscles," *J. Bionic Eng.*, vol. 15, no. 2, pp. 236–246, 2018.

[16] E. Brown et al., "Universal robotic gripper based on the jamming of granular material," *Proc. Nat. Acad. Sci.*, vol. 107, no. 44, pp. 18809–18814, 2010.

[17] N. Cheng et al., "Prosthetic jamming terminal device: A case study of untethered soft robotics," *Soft Robot.*, vol. 3, no. 4, pp. 205–212, Dec. 2016.

[18] T. Hou et al., "Design and experiment of a universal two-fingered hand with soft fingertips based on jamming effect," *Mechanism Mach. Theory*, vol. 133, pp. 706–719, 2019.

[19] J. R. Amend, E. Brown, N. Rodenberg, H. M. Jaeger, and H. Lipson, "A positive pressure universal gripper based on the jamming of granular material," *IEEE Trans. Robot.*, vol. 28, no. 2, pp. 341–350, Apr. 2012.

[20] Y. Wang et al., "Inflatable particle-jammed robotic gripper based on integration of positive pressure and partial filling," *Soft Robot.*, vol. 9, no. 2, pp. 309–323, 2021.

[21] Y. Wei et al., "A novel, variable stiffness robotic gripper based on integrated soft actuating and particle jamming," *Soft Robot.*, vol. 3, no. 3, pp. 134–143, 2016.

[22] M. Fujita et al., "Variable inner volume mechanism for soft and robust gripping—Improvement of gripping performance for large-object gripping," in *Proc. IEEE Int. Symp. Saf., Secur., Rescue Robot.*, 2016, pp. 390–395.

[23] T. Ranzani, M. Cianchetti, G. Gerboni, I. D. Falco, and A. Menciassi, "A soft modular manipulator for minimally invasive surgery: Design and characterization of a single module," *IEEE Trans. Robot.*, vol. 32, no. 1, pp. 187–200, Feb. 2016.

[24] Y. Jiang, D. Chen, C. Liu, and J. Li, "Chain-like granular jamming: A novel stiffness-programmable mechanism for soft robotics," *Soft Robot.*, vol. 6, no. 1, pp. 118–132, Feb. 2019.

[25] Y. Yang, Y. Zhang, Z. Kan, J. Zeng, and M. Y. Wang, "Hybrid jamming for bioinspired soft robotic fingers," *Soft Robot.*, vol. 7, no. 3, pp. 292–308, 2019.

[26] Y. Li, Y. Chen, Y. Yang, and Y. Li, "Soft robotic grippers based on particle transmission," *IEEE/Amer. Soc. Mech. Eng. Trans. Mechatron.*, vol. 24, no. 3, pp. 969–978, Jun. 2019.

[27] A. Jiang, G. Xynogalas, P. Dasgupta, K. Althoefer, and T. Nanayakkara, "Design of a variable stiffness flexible manipulator with composite granular jamming and membrane coupling," in *Proc. IEEE/RSJ Int. Conf. Intell. Robot. Syst.*, 2012, pp. 2922–2927.

[28] R. V. Martinez et al., "Robotic tentacles with three-dimensional mobility based on flexible elastomers," *Adv. Mater.*, vol. 25, no. 2, pp. 205–212, 2013.

Fenglin Han received the B.S. degree in mechanical engineering from Chongqing University, Chongqing, China, in 2004, and the Ph.D. degree in mechanical engineering from the Huazhong University of Science and Technology, Wuhan, China, in 2010.

He is currently an Assistant Professor with State Key Laboratory of Precision Manufacturing for Extreme Service Performance, Central South University, Changsha, China, and also with the College of Mechanical and Electrical Engineering, Central South University, Changsha, China. He is working on the field of soft robotics design and control technologies.

Lei Fei received the B.S. degree in mechanical engineering from Central South University, Changsha, China, in 2019, and the M.S. degree in mechanical engineering from Central South University, Changsha, China, in 2022.

He is working on the field of soft robotics design and soft sensors.

Run Zou received the B.S. degree in mechanical engineering from Central South University, Changsha, China, in 2020. He is currently working toward the M.S. degree in mechanical engineering at Central South University, Changsha, China.

He is working on the field of soft robotics design.

Weijian Li received the B.S. degree in mechanical engineering from Jiangxi University of Science and Technology, Nanchang, Jiangxi, China, in 2020. He is currently working toward the M.S. degree in mechanical engineering at Central South University, Changsha, China.

He is focusing on the field of soft actuators and sensors.

Jinghao Zhou received the B.S. degree in mechanical engineering from Central South University, Changsha, China, in 2020. He is currently working toward the M.S. degree in mechanical engineering at Central South University, Changsha, China.

He is focusing on the field of the applications of control and dynamics in robotic systems.

Haiming Zhao received the B.S. degree from the Department of Mechanics, Central South University of Technology, Changsha, China, in 1988, and the M.S. degree from the Department of Mechanics, Zhejiang University, Hangzhou, China, in 1994.

He is currently a Professor from the State Key Laboratory of Precision Manufacturing for Extreme Service Performance, Central South University, Changsha, China. His research interests include research on deep-sea exploration, and mechanical and electrical integration.

IEEE Transactions on Robotics (T-RO) paper, presented at ICRA 2024, Yokohama, Japan. Cite as T-RO paper.